Control of Harmonic Generation by the Time Delay Between Two-Color, Bicircular Few-Cycle Mid-IR Laser Pulses

M. V. Frolov, N. L. Manakov, A. A. Minina, N. V. Vvedenskii, A. A. Silaev, M. Yu. Ivanov, and Anthony F. Starace

Phys. Rev. Lett. **120**, 263203 — Published 29 June 2018

DOI: 10.1103/PhysRevLett.120.263203

Control of Harmonic Generation by the Time Delay Between Two-Color, Bicircular Few-Cycle Mid-IR Laser Pulses

M.V. Frolov,[1] N.L. Manakov,[1] A. A. Minina,[1] N.V. Vvedenskii,[1,2,3]
A.A. Silaev,[1,2,3] M.Yu. Ivanov,[4,5,6] and Anthony F. Starace[7]

[1] *Department of Physics, Voronezh State University, Voronezh 394018, Russia*
[2] *Institute of Applied Physics, Russian Academy of Sciences, Nizhny Novgorod 603950, Russia*
[3] *University of Nizhny Novgorod, Nizhny Novgorod 603950, Russia*
[4] *Max-Born Institute, Max-Born-Strasse 2A, Berlin D-12489, Germany*
[5] *Blackett Laboratory, Imperial College London, South Kensington Campus, SW7 2AZ London, United Kingdom*
[6] *Department of Physics, Humboldt University, Newtonstrasse 15, 12489 Berlin, Germany*
[7] *Department of Physics and Astronomy, The University of Nebraska, Lincoln NE 68588-0299, USA*

(Dated: June 1, 2018)

We study control of high-order harmonic generation (HHG) driven by time-delayed, few-cycle ω and 2ω counter-rotating mid-IR pulses. Our numerical and analytical study shows that the time delay between the two-color pulses allows control of the harmonic positions, both those allowed by angular momentum conservation and those seemingly forbidden by it. Moreover, the helicity of any particular harmonic is tunable from left- to right-circular without changing the driving pulse helicity. The highest HHG yield occurs for a time delay comparable to the fundamental period $T = 2\pi/\omega$.

High-order harmonic generation (HHG) in a laser field composed of two counter-rotating, circularly-polarized laser beams with frequencies ω and 2ω was pioneered in Refs. [1, 2]. Even though neither circularly-polarized field supports harmonic generation on its own, combining them in a counter-rotating configuration leads to very efficient harmonic emission because ionized electrons undergo field-driven oscillations that return them to the parent ion. This field configuration offers a robust method to generate extreme ultraviolet light with high and tunable ellipticity (see, e.g., Refs. [1–16]), enabling table-top studies of chiral-sensitive light-matter interactions in both gas and condensed phase [6, 8, 10, 17–21].

For counter-rotating bicircular driving pulses, the angular momentum selection rules in spherically symmetric media dictate that the allowed harmonics must have orders $3N+1$ and $3N+2$, while the $3N$–harmonics are forbidden for a long bicircular laser pulse. Orders $3N+1$ (respectively $3N+2$) correspond to the net absorption of $N+1$ (N) ω–photons and N ($N+1$) 2ω–photons. Re-emission of the absorbed photons as a harmonic occurs by radiative recombination to the initial ground state [4], with the emission co-rotating with the ω– (2ω–) field. Orders $3N$ correspond to net absorption of N 2ω–photons and N ω–photons, so that the excited electron state has the same parity as the initial state. Thus, recombination by harmonic emission in this case is forbidden.

In this Letter we show how these simple rules are modified when time-delayed, few-cycle driving pulses are employed. Our theoretical results, obtained both analytically and numerically by solving the 3D time-dependent Schrödinger equation (TDSE), are for laser pulses with fundamental wavelength $\lambda = 2\pi c/\omega = 1.6$ μm and intensity 10^{14} W/cm^2. *First*, we show that for certain time delays between the two driving pulses, the harmonic spectra may be dominated by the "forbidden" $3N$ orders with nearly linear polarization. *Second*, for any given emission frequency we show that one can tune the helicity of the emitted light from nearly circular (right or left) to linear without changing the helicity of the driving laser pulses but by simply tuning the two-color time delay. *Third*, our theoretical analysis of harmonic emission driven by two few-cycle, time-delayed pulses shows the surprising result that the HHG yield is largest for nonzero time delays. Unintuitively, we find the HHG yield increases by an order of magnitude when the two pulses are substantially delayed and relate this phenomenon to the strong dependence of tunneling ionization by a bicircular pulse on the time delay. *Fourth*, even when the two driving pulses barely overlap, electrons liberated by a leading 2ω-pulse can be driven back to the core by the trailing ω-pulse. The different impacts of the ω and 2ω fields on the electron dynamics leads to asymmetric dependence of the harmonic emission on the two-pulse delay time.

To exclude any DC components, our bicircular field $\mathbf{F}(t)$ is defined via an integral of the vector potential $\mathbf{A}(t)$:

$$\int^t \mathbf{A}(\tau)d\tau = \mathbf{R}(t), \quad \mathbf{R}(t) = \mathbf{R}_1(t) + \mathbf{R}_2(t-\mathcal{T}), \qquad (1)$$

$$\mathbf{R}_i = \frac{cF}{\omega_i^2} e^{-2\ln 2 \frac{t^2}{\tau_i^2}} \left(\mathbf{e}_x \cos\omega_i t + \eta_i \mathbf{e}_y \sin\omega_i t\right), \quad i = 1, 2$$

where $\mathbf{A}(t)$ and $\mathbf{F}(t) = -\partial\mathbf{A}(t)/(c\partial t)$ can be found by differentiation (here c is the speed of light), F is the field strength, $\omega_1 = \omega$, $\omega_2 = 2\omega$, η_i is the ellipticity of the ith component ($\eta_1 = -\eta_2 = 1$), and $\tau_i = 2\pi N_i/\omega$ is the duration of the ith pulse (full width at half-maximum in the intensity), which is measured by the number of cycles N_i of the fundamental field. Finally, $\mathcal{T}$ is the time delay between the two pulses, with negative $\mathcal{T}$ corresponding to the 2ω-pulse arriving earlier.

The TDSE was solved numerically for the one-electron potential [expressed in atomic units (a.u.)],

$$U(r) = -\frac{Q(r)}{r} = -\frac{1}{r}\left[\tanh(r/a) + (r/b)\mathrm{sech}^2(r/a)\right],$$

where $a = 0.3$ and $b = 0.461$, using the method described in Refs. [22, 23]. This potential provides a good approximation for the hydrogenic spectrum and smooths the singularity at the origin. This is advantageous for obtaining converged numerical simulations for this wavelength and intensity. However, since numerical simulations become very time-consuming for long wavelengths, an analytical model approach becomes increasingly necessary.

The analytical theory takes advantage of the tunnelling interaction regime in mid-IR fields. In general, the harmonic response can be described in terms of quantum trajectories that obey the classical equations of motion but leave the atom at complex ionization times $\widetilde{t'_j}$ and return at complex recombination times $\widetilde{t_j}$, where j labels the trajectory (see, e.g., Refs. [24–26]). In the tunnelling regime, where the imaginary part of $\widetilde{t'_j}$ is small, $\gamma = \mathrm{Im}\,\omega\widetilde{t'_j} \ll 1$, one can express the emission at frequency Ω via *real* ionization (t'_j) and return (t_j) times. These times obey the following equations [27]:

$$\mathbf{K}'_j \cdot \dot{\mathbf{K}}'_j + \Delta'_j = 0, \quad \mathbf{K}'_j = \mathbf{A}(t'_j)/c + \mathbf{p}(t'_j, t_j), \qquad (2a)$$

$$\mathbf{K}_j^2 + \Delta_j = 2(\Omega - I_p), \quad \mathbf{K}_j = \mathbf{A}(t_j)/c + \mathbf{p}(t'_j, t_j) \qquad (2b)$$

$$\mathbf{p}(t'_j, t_j) = -\int_{t'_j}^{t_j} \mathbf{A}(t)dt/[c(t_j - t'_j)],$$

where I_p is the ionization potential, and $\dot{\mathbf{K}}'_j \equiv \partial \mathbf{K}'_j / \partial t'_j$. The quantum corrections in Eq. (2), Δ'_j and Δ_j, account for the complex-valued parts of the quantum trajectory and are given by the expressions:

$$\Delta'_j = -\frac{1}{6}\left(\frac{\varkappa_j}{\mathcal{F}_j}\right)^2 \dddot{\mathbf{K}'}^2_j, \quad \Delta_j = \left(\frac{\varkappa_j}{\mathcal{F}_j}\right)^2 \frac{\partial^2 {\mathbf{K}'_j}^2}{\partial t'_j \partial t_j},$$

where

$$\varkappa_j = \sqrt{\kappa^2 + {\mathbf{K}'}^2_j}, \quad \mathcal{F}_j = \sqrt{\ddot{\mathbf{K}'}^2_j}, \quad \kappa = \sqrt{2I_p},$$

and $\ddot{\mathbf{K}'}^2_j$, $\dddot{\mathbf{K}'}^2_j$ are second and third derivatives of ${\mathbf{K}'}^2_j$ in t'_j, respectively. Neglecting the quantum corrections, Eq. (2a) ensures that at t'_j the electron has minimal kinetic energy, and Eq. (2b) ensures that the energy gained is converted into a photon of energy Ω upon radiative recombination to the initial bound state with energy $-I_p$.

For each trajectory j, the contribution $\mathbf{d}_j$ to the total induced dipole at a frequency Ω can be written in the factorized form,

$$\mathbf{d}_j = \mathbf{d}_{\mathrm{rec}}(\Omega) P(t_j) \mathcal{W}_j e^{i\mathcal{S}_j} P(t'_j) \mathcal{I}_j(t'_j). \qquad (3)$$

In Eq. (3), the ionization amplitude, $\mathcal{I}_j(t'_j)$, describes the tunneling step of HHG [28] in the adiabatic approximation (see, e.g., Ref. [29]); the propagation factor, $\mathcal{W}_j$, is

$$\mathcal{W}_j = \left[\Delta t_j^{3/2} \sqrt{\mathbf{K}_j \cdot \dot{\mathbf{K}}_j}\right]^{-1}, \qquad (4)$$

where $\Delta t_j = t_j - t'_j$ and $\dot{\mathbf{K}}_j \equiv \partial \mathbf{K}_j / \partial t_j$; the exact recombination dipole is $\mathbf{d}_{\mathrm{rec}}(\Omega) = \mathbf{k}_j f_{\mathrm{rec}}(\Omega)$ ($\mathbf{k}_j = \mathbf{K}_j / |\mathbf{K}_j|$), calculated for the real-valued electron momentum $\mathbf{K}_j$ at the real-valued return time t_j; and the phase $\mathcal{S}_j$ is

$$\mathcal{S}_j = \Omega t_j - \int_{t'_j}^{t_j} \left\{\frac{1}{2}\left[\mathbf{p}(t'_j, t_j) + \mathbf{A}(\xi)\right]^2 + I_p\right\} d\xi. \qquad (5)$$

Finally, the factors $P(t'_j), P(t_j)$ account for ground state depletion at the ionization and recombination times,

$$P(t) = \exp\left(-\frac{1}{2}\int_{-\infty}^{t} \Gamma(|\mathbf{F}(t')|)dt'\right), \qquad (6)$$

where $\Gamma(|\mathbf{F}(t)|)$ is the tunnelling rate in the instantaneous electric field $|\mathbf{F}(t)|$. Since the peak fields may approach the barrier suppression field $F_b = \kappa^4/(16Z)$, we use for Γ the empirical formula of Ref. [30], which differs from the standard tunneling formula of Smirnov and Chibisov [31] by a factor $\exp[-\beta(Z^2/I_p)(F/\kappa^3)]$, where $\beta = 5.6$ is a fitting parameter and $Z = 1$ is the core charge.

The numerical TDSE results and the analytic theory results for the harmonic spectrum and the degree of circular polarization for $\mathcal{T} = 0$ are compared in Figs. 1(a,b), demonstrating excellent agreement for the higher energy parts of the HHG spectra. Discrepancies are only found for low harmonics with $\Omega < u_p = F^2/(4\omega^2)$ (not shown in Fig. 1), i.e., for very short trajectories, where the adiabatic three-step picture appears to fail.

Note that the harmonic spectrum in Fig. 1(a) does not show the usual spectral structure characteristic of an $\omega - 2\omega$ counter-rotating bicircular field, with allowed harmonic pairs $3N + 1$ and $3N + 2$ and missing (forbidden) $3N$ harmonics for each integer N. Instead, we see an oscillation pattern typical of the interference of *two* emission bursts, suggesting a simple means to control both the spectra and the ellipticities of the harmonics.

The short duration of our two-color, counter-rotating laser pulses results in a kind of ionization gating that fa-

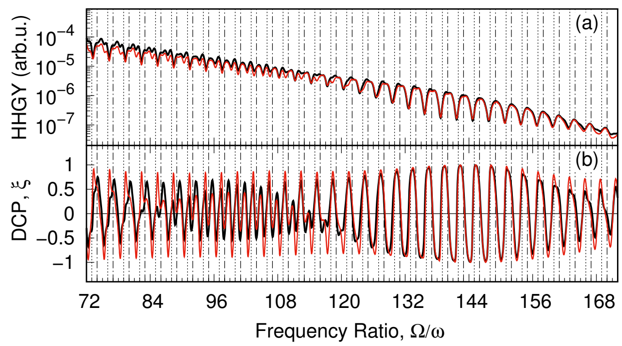

Figure 1. Comparison of TDSE results (thin black lines) with results of the analytical adiabatic approach (thin red lines) for the HHG spectral yield (HHGY) (top) and harmonic degree of circular polarization (DCP) ξ (bottom) for a counter-rotating $\omega - 2\omega$ bicircular field (1) with fundamental wavelength $\lambda \equiv 2\pi c/\omega = 1.6$ μm. Calculations were done for the H atom for zero time delay ($\mathcal{T} = 0$) between two-color 3-cycle pulses ($N_1 = N_2 = 3$), each having a peak field strength $F = 0.0534$ a.u. (or an intensity $I = 10^{14}$ W/cm^2).

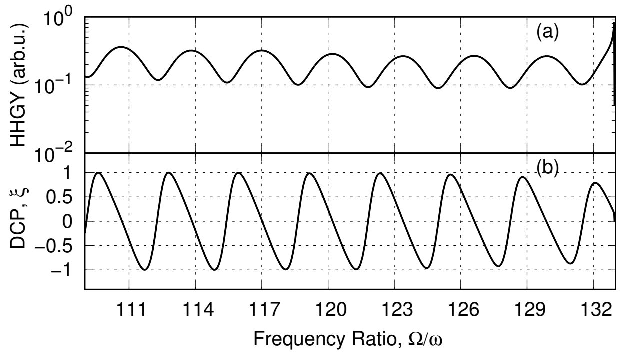

Figure 2. Time-delay control of the HHG spectrum: (a) harmonic yield; (b) degree of circular polarization ξ. The spectrum contains almost exclusively linearly-polarized "forbidden" $3N$ harmonic (see H114, H117, H120) and an "allowed" $3N+1$ harmonic (H130). Results are for the H atom and the bicircular field (1) with intensity $I = 10^{14}$ W/cm^2 for each component, $N_1 = N_2 = 2$, $\mathcal{T} = -2\pi/\omega$, and $\lambda = 1.6$ μm.

vors only two ionization trajectories for harmonic emission (i.e., only two partial $\mathbf{d}_j$ contribute significantly). Consequently, a model of two emitting dipoles, discussed below, is suitable for the physical interpretation of our results. Let a harmonic frequency Ω be generated by two dipoles, $\mathbf{d}_1 e^{-i\Omega t}$ and $\mathbf{d}_2 e^{-i(\Omega t+\Phi)}$, where $\mathbf{d}_1$ and $\mathbf{d}_2$ are *real* vectors and Φ is their relative phase. While each individual dipole emits linearly polarized light, their superposition does not. If α is the physical angle between the two dipoles, then the degree of circular polarization, ξ, of the emitted radiation is given by (see Ref. [32]):

$$\xi = -\frac{\sin\alpha \sin\Phi}{\delta + \cos\alpha\cos\Phi}, \quad \delta = \frac{d_1^2 + d_2^2}{2d_1 d_2}. \tag{7}$$

Equation (7) shows that ξ can be varied in the range $(-1/\delta; 1/\delta)$ by varying the relative phase Φ between the two dipoles, with full control of ξ available for $\delta \simeq 1$. For a bicircular driving field, the relative phase Φ is controlled by changing the time delay between the two driving colors, which controls the electron trajectories responsible for a given emission frequency.

The oscillation patterns in Fig. 1(b) confirm this analysis. The phase between the two dipoles in Eq. (7) is $\Phi = \mathcal{S}_1 - \mathcal{S}_2$, and α is the angle between the vectors $\mathbf{K}_1$ and $\mathbf{K}_2$ – the electron velocities for the two dominant recombination events. For the bicircular field, $\alpha \simeq 120°$ or $2\pi/3$. For $\delta = 1$, circularly polarized light is emitted for $\Phi = \pi \pm \alpha$, with "+" for $\xi = +1$ and "−" for $\xi = -1$. Since Φ is of order $F^2/\omega^3 \gg 1$, it results in a rapid oscillation pattern in $\xi(\Omega)$ between the maximum and minimum values, as seen in Fig. 1(b). On the other hand, for $\alpha \simeq 2\pi/3$, the maxima of the total harmonic yield occur for $\Phi = \mathcal{S}_1 - \mathcal{S}_2 = \pi + 2\pi\nu$ (for integer ν), i.e., the interference peaks in the total yield are offset from the maxima in ξ, as shown in Figs. 1 and 2.

This simple physical model indicates the possibility of controlling the HHG spectrum and the harmonic ellipticities: e.g., two dominant emission bursts separated by approximately one-third of an optical cycle may yield a region of the HHG spectrum with single peaks at $3N\omega$ [33], in stark contrast with the usual HHG spectrum for a bicircular field. Using the analytic approach, this result is shown in Fig. 2 for a time delay between the two pulses of $\mathcal{T} = -T$. However, as the time between successive emission bursts is only approximately $T/3$, we observe some shifts in the positions of interference maxima and degrees of circular polarization. Thus for a pulsed bicircular field, $3N\omega$ peaks with nearly linear polarization can be observed only in particular ranges of harmonic energies (e.g., $114 \le \Omega/\omega \le 120$ in Fig. 2); also, "allowed" $3N+1$ harmonics with linear (instead of circular) polarization can be observed (e.g., $\Omega/\omega = 130$ in Fig. 2).

For any Ω (or return electron energy $E = \Omega - I_p$), the analytic theory can trace the main contributing closed electron trajectories given by Eq. (2). They are described by the classical equations of motion, except that the real-valued ionization and recombination times include quantum corrections. In Fig. 3 we present the dependence of the electron return energy E in units of $u_p = F^2/4\omega^2$, $\varepsilon = E/u_p$, as a function of the ionization time, t'_j, and the travel time, Δt_j. The gradually changing colors along the steeply-sloped curves in Fig. 3 indicate the relative contribution of the classical trajectory at each t'_j, which is governed by the ionization factor $\mathcal{I}_j$. (The dependence of the ionization factor on the recombination time is given in Ref. [33].) In contrast to the case of linear polarization [see Fig. 3(f)], for a time-delayed few-cycle, bicircular field there are two pronounced ionization bursts at times t'_j governed by the time delay [see Figs. 3(a)-(e)]. Moreover, the dominant trajectories for time-delayed few-cycle counter-rotating bicircular fields (see Fig. 3 of Ref. [33]) are markedly different from those for a linearly polarized pulse or for a long bicircular field [2].

For a large negative delay ($-3T$) equal to the duration of the fundamental pulse [see Fig. 3(a)], one might expect significantly reduced harmonic emission. Unexpectedly, there is surprisingly strong emission from *very long* trajectories returning to the atom with high energy $\varepsilon \approx 2$ after nearly 3 optical cycles, while short trajectories contribute for energies $\varepsilon < 1.5$. For small negative delays and all positive delays, *very long* trajectories do not contribute; trajectories with travel time less than an optical period determine the shape and cutoff of the HHG spectrum. For zero delay, the HHG yield is about an order of magnitude smaller than for negative delays [33].

There is thus no symmetry between large positive and negative delays: for large positive delays the long trajectories remain suppressed and the harmonic spectra are dominated by the short trajectories, which start and finish during the time the two pulses overlap. This difference becomes clear upon noting that both the drift velocity and the lateral displacement of trajectories in the fundamental field are larger than those in the second harmonic field: the displacement in the ω–pulse is about four times larger than in the 2ω–pulse. Thus, for large time delays returning to the origin is possible when the delayed

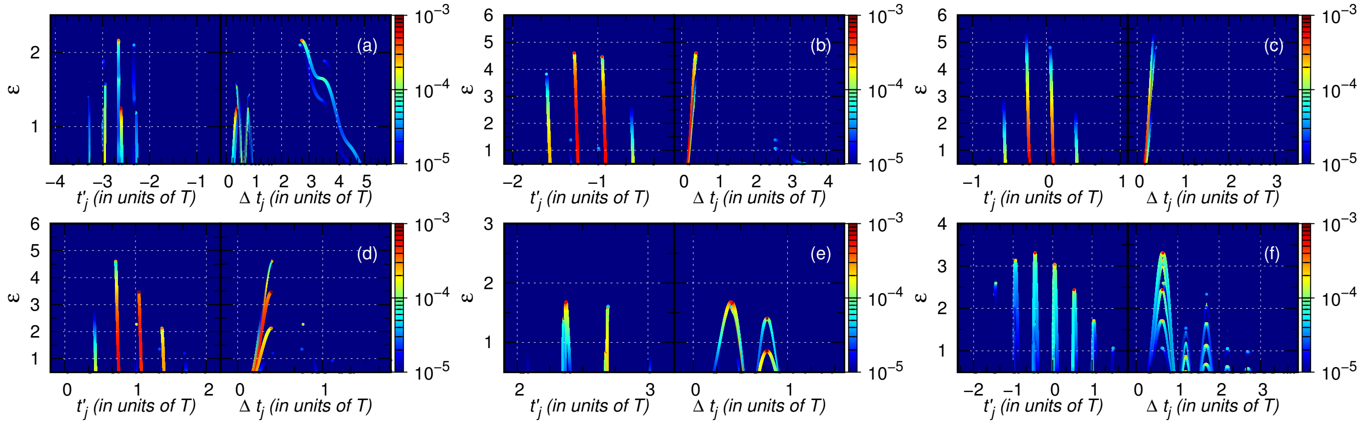

Figure 3. Dependence of the scaled return energy, $\varepsilon = E/u_p$, where $u_p = F^2/(4\omega^2)$, on the jth trajectory's ionization time, t'_j, and travel time, Δt_j, for five time delays $\mathcal{T}$ (in units of $T \equiv 2\pi/\omega$) between the two driving pulses: (a) $\mathcal{T} = -3T$; (b) $\mathcal{T} = -T$; (c) $\mathcal{T} = 0$; (d) $\mathcal{T} = T$; (e) $\mathcal{T} = 3T$. For reference, panel (f) shows the spectrum for a single-color linearly-polarized field. Results are for the H atom and laser parameters $I = 10^{14}$ W/cm^2, $\lambda = 1.6$ μm, $N_1 = 3$, and $N_2 = 2$. The color scale shows the relative contributions of the dipoles, $\propto |\mathbf{d}_j|^2$.

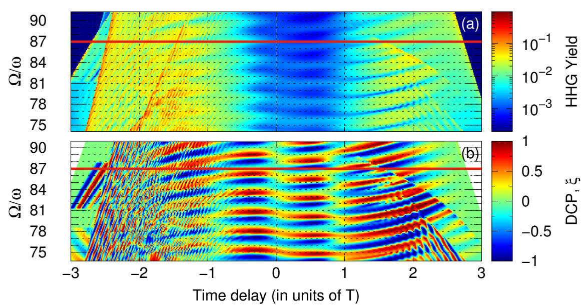

Figure 4. Color-coded emission intensities (a) and degree of circular polarization ξ (b) vs. two-color pulse time delay, $\mathcal{T}$, and emission energy, Ω. The laser parameters are the same as in Fig. 3. Discontinuities in panels (a,b) occur when the second order time-derivative of the classical action goes through zero, $\mathbf{K}_j \cdot \dot{\mathbf{K}}_j = 0$, leading to the inapplicability of Eq.(3). Results for $N = 87$ [solid (red) lines] are plotted in Fig. 5.

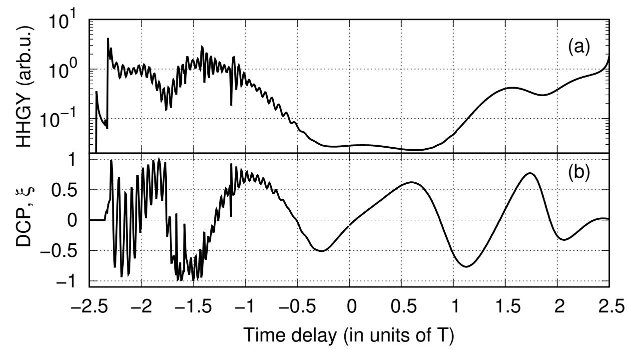

Figure 5. Dependence of the HHG yield (a) and degree of circular polarization ξ (b) on the time delay, taken from Fig. 4 for harmonic energy $\Omega = 2.48$ a.u. ($N = 87$). For this energy, the analytic theory cannot be applied for $|\mathcal{T}| \gtrsim 2.5T$ since there are no real solutions of Eq. (2).

ω-pulse drives back the electron initially launched by the 2ω–pulse, but not vice versa. The trajectory analysis shows that positive time delays allow for easier control of emission properties, since only a few trajectories (with travel times less than a period T) contribute.

Our trajectory analysis is confirmed in Fig. 4, which maps the harmonic intensities and polarizations as a function of the time delay (see also [33]). A rich interference structure is observed up to $\mathcal{T} = -0.5T$, with large-scale and fine-scale oscillations (see also Fig. 5). The origin of large- and fine-scale oscillations can be understood by analysing the phase difference between two trajectories, which may be approximately presented as a linear function [see Eq. (5)]: $\Phi = \mathcal{S}_1 - \mathcal{S}_2 \approx \Omega(t_1 - t_2) + c_0$, where c_0 is approximately constant. The interference of two trajectories with close return times (e.g., $t_1 - t_2 \approx T/3$) leads to large-scale oscillations, whereas interference of trajectories with very different return times (e.g., $t_1 - t_2 \geq T$) leads to fine-scale oscillations. Since for positive time delays the trajectories do not have large differences in their recombination times, the HHG spectra and polarization properties depend smoothly on the time delay.

Figures 4(a) and 5(a) confirm the suppression of the HHG yield for close to zero two-pulse delay and its enhancement for both positive and negative $\mathcal{T}$. Such HHG yield behavior is consistent with the suppression and enhancement of ionization with changing time delays between the two pulses (see Fig. 3 and Fig. 1 in Ref. [33]). Figures 4(b) and 5(b) confirm the ability to control the ellipticity of a given emission frequency as a function of the two-color time delay, as predicted by the simple physical model of two dominant emission bursts.

To conclude, based on the proposed theoretical approach for HHG driven by a few-cycle, counter-rotating bicircular laser field, we have shown that the waveform can be sculpted by means of the time delay between pulses to efficiently control HHG intensities and polarizations. This time-delay scheme has also been shown to allow generation of the seemingly forbidden $3N$ harmonics, in sharp contrast with the case of long-pulse bicircular fields. Finally, as demonstrated above, the helicity of the generated harmonics can be continuously varied from -1 to $+1$ by changing the time delay between the two-color pulses, thus indicating that this time delay scheme is an efficient means to control harmonic polarizations.

This work was supported in part by the Ministry of Education and Science of the Russian Federation through Grant No. 3.1659.2017/4.6, the Russian Science Foundation through Grant No. 18-12-00476 (numerical calculations), and by the U.S. National Science Foundation through Grant No. PHY-1505492 (A.F.S.). M. I. acknowledges the support of the DFG QUTIF grant.

[1] H. Eichmann, A. Egbert, S. Nolte, C. Momma, B. Wellegehausen, W. Becker, S. Long, and J. K. McIver, Phys. Rev. A **51**, R3414 (1995).
[2] D. B. Milošević, W. Becker, and R. Kopold, Phys. Rev. A **61**, 063403 (2000).
[3] A. Fleischer, O. Kfir, T. Diskin, P. Sidorenko, and O. Cohen, Nat. Photon. **8**, 543 (2014).
[4] M. Ivanov and E. Pisanty, Nat. Photon. **8**, 501 (2014).
[5] E. Pisanty, S. Sukiasyan, and M. Ivanov, Phys. Rev. A **90**, 043829 (2014).
[6] O. Kfir, P. Grychtol, E. Turgut, R. Knut, D. Zusin, D. Popmintchev, T. Popmintchev, H. Nembach, J. M. Shaw, A. Fleischer, H. Kapteyn, M. Murnane, and O. Cohen, Nat. Photon. **9**, 99 (2015).
[7] A. Ferré, C. Handschin, M. Dumergue, F. Burgy, A. Comby, D. Descamps, B. Fabre, G. A. Garcia, R. Géneaux, L. Merceron, E. Mével, L. Nahon, S. Petit, B. Pons, D. Staedter, S. Weber, T. Ruchon, V. Blanchet, and Y. Mairesse, Nat. Photon. **9**, 93 (2015).
[8] D. D. Hickstein, F. J. Dollar, P. Grychtol, J. L. Ellis, R. Knut, C. Hernández-García, D. Zusin, C. Gentry, J. M. Shaw, T. Fan, K. M. Dorney, A. Becker, A. Jaroń-Becker, H. C. Kapteyn, M. M. Murnane, and C. G. Durfee, Nat. Photon. **9**, 743 (2015).
[9] L. Medišauskas, J. Wragg, H. van der Hart, and M. Yu. Ivanov, Phys. Rev. Lett. **115**, 153001 (2015).
[10] T. Fan, P. Grychtol, R. Knut, C. Hernández-García, D. D. Hickstein, D. Zusin, C. Gentry, F. J. Dollar, C. A. Mancuso, C. W. Hogle, O. Kfir, D. Legut, K. Carva, J. L. Ellis, K. M. Dorney, C. Chen, O. G. Shpyrko, E. E. Fullerton, O. Cohen, P. M. Oppeneer, D. B. Milošević, A. Becker, A. A. Jaroń-Becker, T. Popmintchev, M. M. Murnane, and H. C. Kapteyn, Proc. Nat. Acad. Sci. USA **112**, 14206 (2015).
[11] D. Baykusheva, M. S. Ahsan, N. Lin, and H. J. Wörner, Phys. Rev. Lett. **116**, 123001 (2016).
[12] C. Hernández-García, C. G. Durfee, D. D. Hickstein, T. Popmintchev, A. Meier, M. M. Murnane, H. C. Kapteyn, I. J. Sola, A. Jaron-Becker, and A. Becker, Phys. Rev. A **93**, 043855 (2016).
[13] O. Kfir, P. Grychtol, E. Turgut, R. Knut, D. Zusin, A. Fleischer, E. Bordo, T. Fan, D. Popmintchev, T. Popmintchev, H. Kapteyn, M. Murnane, and O. Cohen, J. Phys. B **49**, 123501 (2016).
[14] S. Odžak, E. Hasović, and D. B. Milošević, Phys. Rev. A **94**, 033419 (2016).
[15] A. D. Bandrauk, F. Mauger, and K.-J. Yuan, J. Phys. B **49**, 23LT01 (2016).
[16] Á. Jiménez-Galán, N. Zhavoronkov, M. Schloz, F. Morales, and M. Ivanov, Opt. Expr. **25**, 22880 (2017).
[17] C. D. Stanciu, F. Hansteen, A. V. Kimel, A. Kirilyuk, A. Tsukamoto, A. Itoh, and Th. Rasing, Phys. Rev. Lett. **99**, 047601 (2007).
[18] A. L. Cavalieri, N. Müller, Th. Uphues, V. S. Yakovlev, A. Baltuška, B. Horvath, B. Schmidt, L. Blümel, R. Holzwarth, S. Hendel, M. Drescher, U. Kleineberg, P. M. Echenique, R. Kienberger, F. Krausz, and U. Heinzmann, Nature (London) **449**, 1029 (2007).
[19] J.-Y. Bigot, M. Vomir, and E. Beaurepaire, Nat. Phys. **5**, 515 (2009).
[20] R. Cireasa, A. E. Boguslavskiy, B. Pons, M. C. H. Wong, D. Descamps, S. Petit, H. Ruf, N. Thiré, A. Ferré, J. Suarez, J. Higuet, B. E. Schmidt, A. F. Alharbi, F. Légaré, V. Blanchet, B. Fabre, S. Patchkovskii, O. Smirnova, Y. Mairesse, and V. R. Bhardwaj, Nat. Phys. **11**, 654 (2015).
[21] O. Kfir, S. Zayko, C. Nolte, M. Sivis, M. Möller, B. Hebler, S. S. P. K. Arekapudi, D. Steil, S. Schäfer, M. Albrecht, O. Cohen, S. Mathias, and C. Ropers, Science Adv. **3**, eaao4641 (2017).
[22] T. S. Sarantseva, A. A. Silaev, and N. L. Manakov, J. Phys. B **50**, 074002 (2017).
[23] M. V. Frolov, N. L. Manakov, T. S. Sarantseva, A. A. Silaev, N. V. Vvedenskii, and A. F. Starace, Phys. Rev. A **93**, 023430 (2016).
[24] M. Lewenstein, P. Balcou, M. Yu. Ivanov, A. L'Huillier, and P. B. Corkum, Phys. Rev. A **49**, 2117 (1994).
[25] P. Salières, B. Carré, L. Le Déroff, F. Grasbon, G. G. Paulus, H. Walther, R. Kopold, W. Becker, D. B. Milošević, A. Sanpera, and M. Lewenstein, Science **292**, 902 (2001).
[26] D. B. Milošević, D. Bauer, and W. Becker, J. Mod. Opt. **53**, 125 (2006).
[27] A. A. Minina, M. V. Frolov, A. N. Zheltukhin, and N. V. Vvedenskii, Quant. Electron. **47**, 216 (2017).
[28] P. B. Corkum, Phys. Rev. Lett. **71**, 1994 (1993).
[29] M. V. Frolov, N. L. Manakov, A. A. Minina, S. V. Popruzhenko, and A. F. Starace, Phys. Rev. A **96**, 023406 (2017).
[30] X. M. Tong and C. D. Lin, J. Phys. B **38**, 2593 (2005).
[31] B. M. Smirnov and M. I. Chibisov, Zh. Eksp. Teor. Fiz. **49**, 841 (1965) [Sov. Phys. JETP **22**, 585 (1966)].
[32] L. D. Landau and E. M. Lifshitz, *The Classical Theory of Fields*, 4th ed. (Pergamon, Oxford, 1994).
[33] See Supplemental Material at [URL will be inserted by publisher] for (1) a derivation showing how the $\Omega = 3N\omega$ harmonics in Fig. 2 can appear in the HHG spectra for few-cycle time-delayed, counter-rotating two-color pulses; (2) the dependence of the ionization factor on

the recombination time for seven different time delays between the two-color pulses; and (3) plots of the HHG spectra corresponding to the trajectories in Fig. 3 for five different time-delays between the two-color pulses and an illustration of closed classical electron trajectories for three different time delays.